ACS OMEGA

http://pubs.acs.org/journal/acsodf

Article

Experimental Study on Thermal-Induced Runaway in High Nickel Ternary Batteries

Longzhou Jia, Dong Wang, Tao Yin, Xichao Li, Liwei Li, Zuoqiang Dai,* and Lili Zheng*

Cite This: *ACS Omega* 2022, 7, 14562−14570

Read Online

ACCESS | Metrics & More | Article Recommendations

ABSTRACT: Recently, fire and explosion accidents associated with lithium ion battery failure occurred frequently. Safety has become one of the main constraints on the wide application of lithium ion batteries in the field of electric vehicles (EVs). By using a simultaneous thermal analyzer (STA8000) and accelerating rate calorimetry (ARC), we studied the thermal stability of high nickel battery materials and the high temperature thermal runaway of the battery, combining the two experimental results to analyze the battery thermal runaway process. We studied the temperature difference between inside and outside during thermal runaway by arranging two temperature sensors inside and outside the battery. The chemical reactions of the battery at high temperature through the thermal performance of the anode, cathode, and separator are also revealed. In-depth exploration of the occurrence process and the trigger mechanism of thermal runaway of lithium batteries was made. The main findings of the study are as follows: The temperature at which the anode materials begin to decompose is 77.13 °C, caused by decomposition of the solid electrolyte interface and the temperature at which the cathode materials begin to decompose is 227.09 °C. The maximum surface temperature of the battery during thermal runaway is 641.41 °C; and the maximum inside temperature of the battery is 1117.80 °C. The time difference between the maximum temperatures inside and outside the battery is 40 s. The thermal runaway temperature of the battery T_c is 228.47 °C, which is mainly contributed by the internal short circuit of the anode and cathode to release Joule heat and the cathode/electrolyte reaction. The maximum temperature of T_m is 642.65 °C, which is mainly caused by the reaction between oxygen and electrolyte.

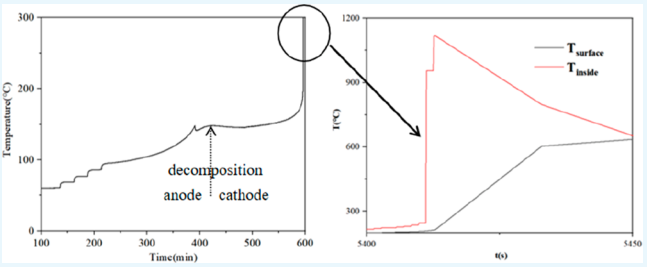

1. INTRODUCTION

Lithium ion batteries have been widely used in electric vehicles, hybrid electric vehicles, energy storage grids, and other items because of their high energy density, high working voltage platform, lack of memory effect, low self-discharge rate, and long service life.[1−3] However, in recent years, lithium ion battery thermal runaway has occurred frequently due to vehicle fires, explosions, and other accidents. Battery safety has become a key issue limiting lithium ion battery development.[4]

The main triggers of thermal runaway of lithium batteries are caused by (1) metal particles left in batteries during the manufacturing process that pierce the diaphragm; (2) high-temperature thermal abuse, causing battery separators to melt and make contact with the cathode and anode materials; (3) electrical abuse, such as overcharging or overdischarging caused by Li (Cu) dendrites piercing the separator; and (4) mechanical abuse, whereby batteries are used in ways involving needles or extrusions.

Feng[5] used a time series diagram to examine the connection between battery material reactions at a high temperature and the thermal characteristics of battery monomers. Macroscopically, three smoke/fire phenomena can be observed during battery thermal runaway: grayish-white smoke caused by the vaporization of dimethyl carbonate and ethyl mercaptan in the electrolyte at high temperature, grayish-white smoke caused by ethylene carbonate (EC) vaporization in the electrolyte, and black smoke due to the melting of the Al collector and C_xH_y generated by combustion. Microscopically, batteries heat up sequentially through the solid electrolyte interface (SEI) membrane decomposition reaction, the reaction of the embedded lithium anode with the electrolyte, the melting of the diaphragm, and the reaction of the positive electrode with the electrolyte.[6,7]

The first release of heat from a high-temperature battery comes from the anode. Feng divided the exothermic reaction of the anode material into three stages.[8,9] The initial stage is the exothermic decomposition of the SEI film on the anode surface, which was observed previously to exist at temperatures

Received: November 18, 2021
Accepted: April 7, 2022
Published: April 19, 2022

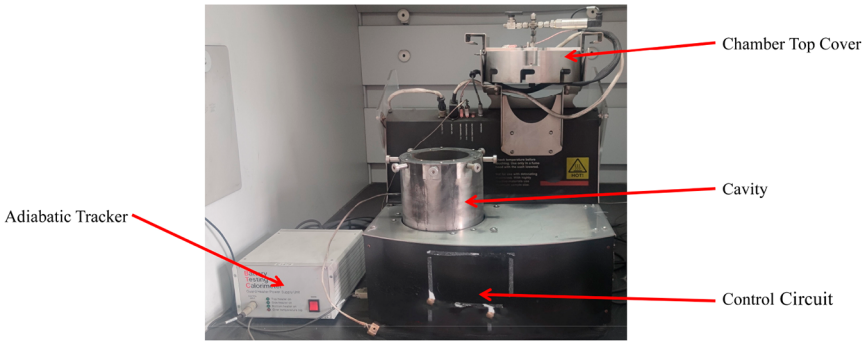

(a) BTC130 calorimeter

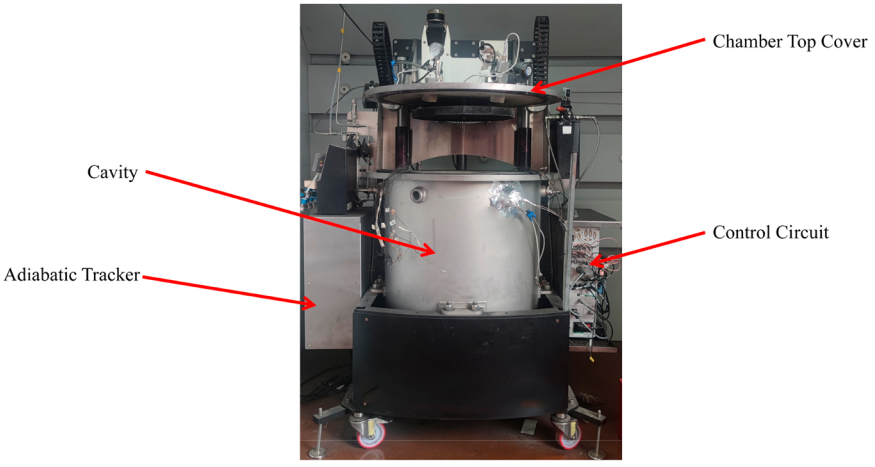

(b) BTC500 calorimeter

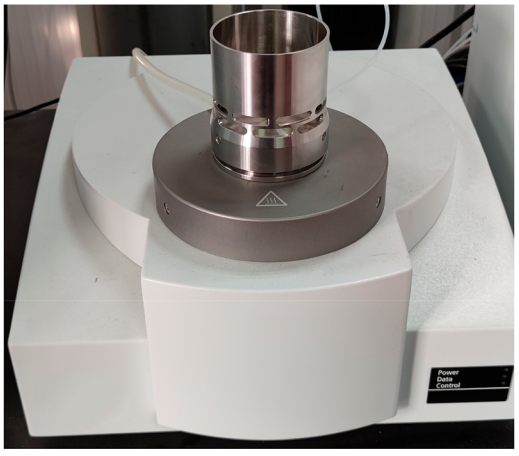

(c) STA8000synchronous calorimeter

Figure 1. Test equipment: (a) BTC130 calorimeter; (b) BTC500 calorimeter; (c) STA8000 synchronous calorimeter.

ranging from 57 to 250 °C. The third exothermic stage is the reaction of the anode decomposition with the electrolyte, which occurs at a temperature greater than 250 °C. Between these stages is the second, where the reaction of regenerating the SEI film occurs at the anode electrode after the thickness reduction due to the decomposition of the SEI film during the first stage.[10] The decomposition and regeneration of SEI membranes reach a balance in this exothermic stage, which has a wide temperature range and a stable exothermic rate.

The separator undergoes a process of shrinking, fusing, and collapsing as the temperature rises. The collapse of the separator causes a large area internal short circuit. The released Joule heat causes the battery to heat up quickly and directly trigger a thermal runaway. The temperature of the internal short circuit is related to the separator material. The melting points of polyethylene (PE) and polypropylene (PP) diaphragms are about 130 and 170 °C, respectively, and the melting point of the ceramic separator can reach 257 °C.[11] The cathode materials undergo a decomposition reaction at a high temperature with an exothermic peak that is generally higher than 200 °C. The oxygen precipitated by the reaction reacts with the electrolyte to release a large amount of heat.[12]

Doughty[13,14] has pioneered the use of accelerating rate calorimetry (ARC) to investigate the thermal runaway (TR)

https://doi.org/10.1021/acsomega.1c06495
ACS Omega 2022, 7, 14562−14570

behaviors of 18650 lithium ion batteries and summarized possible exothermic reactions inside a battery at different stages of the TR process. Golubkov[15] studied the thermal stability of different types of 18650 lithium ion batteries and found that higher battery energy densities were inversely proportional to safety performance. Ping[16] believed that, as the state of charge (SOC) decreased, the peak heat release rate, battery heating, and mass loss would also decrease. Kong[17] established a three-dimensional model to study the effects of battery materials, external heating conditions, and heat dissipation conditions on the thermal runaway of a battery. The results show that the increase in the melting temperature of the separator can increase the onset temperature of thermal runaway and delay the occurrence of thermal runaway. Jhu[18] used a vent sizing package 2 (VSP2) adiabatic calorimeter to study the high-temperature thermal runaway of a battery, finding that the starting temperature of heat release for a commercial 18650 battery is about 140 °C, the trigger temperature of thermal runaway is about 200 °C, and the highest temperature reachable during thermal runaway is 733 °C. Duh[19] conducted safety tests on various commercial 18650 lithium ion batteries under 100% SOC, finding that the average self-exothermic onset temperature of such a battery was 159.1 ± 8.3 °C and the maximum thermal runaway temperature was 498.4 ± 25.6 °C. Zhu[20] established the thermal abuse model of a lithium ion battery and analyzed and compared the thermal runaway characteristics of the battery oven test and the battery under the condition of local heating. The test results show that, if the battery is locally heated and the heating area is small, the battery will not be thermally runaway. Sun[21] investigated the thermal runaway behaviors of lithium ion batteries with $LiNi_{0.6}Co_{0.2}Mn_{0.2}O_2$ and $LiNi_{0.8}Co_{0.1}Mn_{0.1}O_2$ cathode materials, finding that the onset temperature of thermal runaway for the battery with the $LiNi_{0.8}Co_{0.1}Mn_{0.1}O_2$ cathode is 20 °C lower than that with the $LiNi_{0.6}Co_{0.2}Mn_{0.2}O_2$ cathode, demonstrating that battery thermal runaway is highly correlated with cathode chemistry. Li[22] investigated the TR behavior of a lithium ion battery triggered by a cylindrical heater. The effects of state of charge (SOC), the power of the heater, and the cell spacing were studied, and the amount of heat transferred between the cell and the heater was calculated. Li[23] investigated the thermal runaway mechanism of an $LiNi_{0.8}Co_{0.1}Mn_{0.1}O_2$ based lithium ion battery. The reaction between the cathode and flammable electrolyte was proved to be the trigger of the thermal runaway accident. Liu[24] investigated the effects of the SOC and the charging−discharging process on the thermal runaway of 18650 lithium ion batteries, finding that the thermal runaway initial temperature of the lithium ion battery decreases with the increasing SOC. Zhang[25] investigated the thermal runaway behavior of the NCM ternary lithium ion battery in hot and high humidity environment, analyzing on the basis of tests and simulations and finding that a hot and high relative humidity environment has a significant enhancement effect on the risk of the thermal runaway of the NCM lithium ion battery. Wang[26] used an accelerating rate calorimeter (ARC) to study the thermal runaway of 37 Ah NCM111, 50 Ah NCM523, and 50 Ah NCM622 batteries. The self-exothermic onset temperatures were 90.9, 71.2, and 69.6 °C, respectively; the thermal runaway trigger temperatures were 241.1, 244.1, and 248.4 °C, respectively; the maximum thermal runaway temperatures were 958.5, 964.3, and 1009.2 °C, respectively; and the ΔH values were 645 084 J, 706 600 J, and 780 014 J, respectively. Wang[27] used ARC to study the high-temperature thermal runaway of a 23 Ah NCM523 soft-pack battery. The 75% SOC battery showed a large bulge near the positive electrode at 171.06 °C, and the battery temperature rise rate was 2.53 °C/min. Zhao[28] used the ARC ramp heating test method to study the thermal runaway of an 18650 battery. The maximum thermal energy released at 100% SOC was 61.72 kJ (equivalent to 5.57 g of TNT), the maximum runaway temperature was 727.64 °C, the maximum peak pressure was 36.33 bar, and the maximum gas volume was 116.58 mmol.

This work first investigates the thermal stabilities of battery materials through heat flow and thermogravimetric curves and then explores heat generation in a battery. Second, by arranging two temperature sensors inside and outside a battery, respectively, we explore the temperature difference between the inside and the surface of the battery during high-temperature thermal runaway. Finally, the characteristics of thermal runaway behavior caused by heating are studied, and then the depth of the mechanism of high-temperature thermal runaway in lithium batteries is revealed. This paper is important to provide guidance on the prevention, control, and early warning of thermal runaway.

2. EXPERIMENTAL DESIGN

2.1. Test Equipment. The ARC provides an adiabatic environment for the test sample. It is mainly used to obtain reaction kinetics and thermodynamic parameters of test samples so that risk can be evaluated. The ARCs used in this study are the BTC130 and BTC500 calorimeters produced by H.E.L Group (U.K.). Figure 1a shows the BTC130 calorimeter, and Figure 1b shows the BTC500 calorimeter. The temperature accuracy is 0.01 °C. The STA8000 synchronous calorimeter, shown in Figure 1c and made by PerkinElmer (USA) can test a sample's thermogravimetric and calorimetric/differential thermal signals simultaneously.

2.2. Test Battery. The test object in this article is a commercial 18650 high nickel battery (made in Guang Dong Province, China), the anode material is graphite, and the rated capacity of the battery is 2.9 Ah. The specific battery information is shown in Table 1. Before testing started, five charge−discharge cycles were performed at 25 °C with a standard charge−discharge rate to stabilize the battery. The battery consistency is good, and follow-up tests can be carried out. Figure 2 shows the actual battery diagram and the battery disassembly diagram.

Table 1. Battery Information

parameter	value
anode	graphite
cathode	$Li(Ni_{0.8}Co_{0.1}Mn_{0.1})O_2$
separator	PP/PE/PP (three layers)
electrolyte	$LiPF_6$/DMC:EMC:EC = 1:1:1
rated capacity	2.9 Ah
operating voltage	2.5−4.2 V
weight	47−48 g

2.3. Test Methods. *2.3.1. Test Method for Battery Material Thermal Stability.* Disassemble the 100% SOC high nickel battery in the glovebox, separate the cathode, anode, and separator of the battery, and then dry them in a ventilated place for 24 h. Scrape about 10−30 mg of battery material from the electrode current collector of the battery and

https://doi.org/10.1021/acsomega.1c06495
ACS Omega 2022, 7, 14562−14570

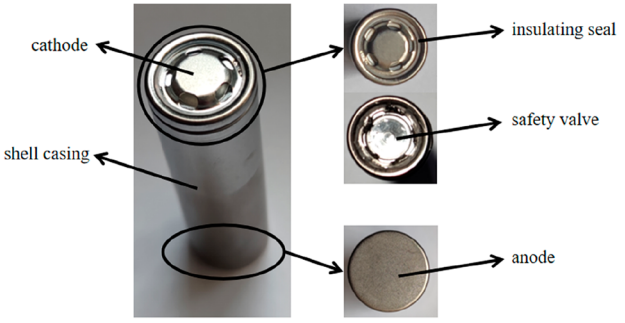

(a) actual battery

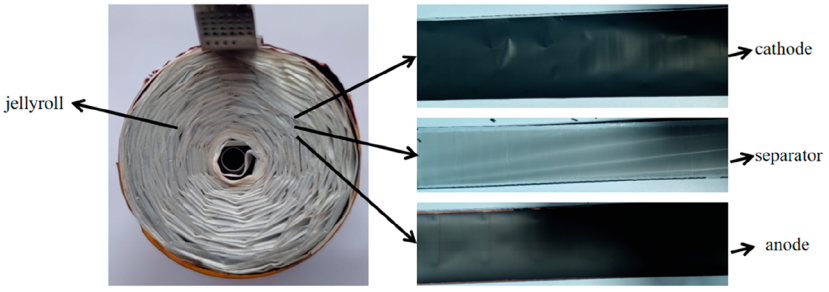

(b) battery disassembly diagram

Figure 2. (a) Actual battery and (b) battery disassembly diagrams.

put it into the STA8000. Set the temperature rise range of the instrument to 50−900 °C and the temperature rise rate to 10 °C/min. Start the experiment.

2.3.2. Test Method for Temperature Difference between Inside and Outside of Battery. Use a tool to open the safety valve and insulating pad of the 100% SOC battery, revealing the material winding structure of the battery and the core shaft at the center. Pull out the core shaft and paste a temperature sensor to the middle of the core shaft with thermal insulation tape. Insert the mandrel into the core, and arrange a temperature sensor on the outer surface of the battery (as shown in Figure 3). Seal the safety valve with high-temperature tape. Finally, start the ARC "ramp" program to heat the battery to thermal runaway.

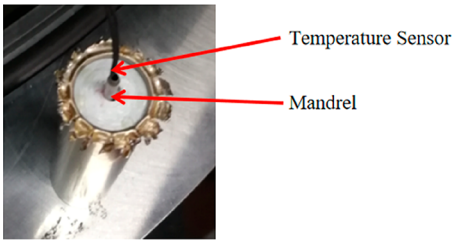

Figure 3. Arrangement of temperature sensor for battery spindle.

The ARC ramp program triggers the battery thermal runaway by means of external heat induction. The test principle is that the ARC cavity heats up according to the set temperature rise rate, transferring heat to the battery through air convection so that the battery heats up until thermal runaway or the test cutoff temperature is reached. The ramp program parameter settings are shown in Table 2.

2.3.3. Test Method for High Temperature Thermal Runaway of a Battery Cell. The ARC's "heat−wait−search" (HWS) program is used to study the high-temperature thermal runaway of battery cells. The test principle is as follows: at the beginning of the test, the battery is heated to the starting temperature of the experiment; after that, the calibration stage begins; the calibration phase continues to ensure the battery heats evenly; then the "wait" mode starts so that the battery and cavity reach thermal equilibrium; after the wait mode is over, the "search" stage begins and the system judges whether the battery will start to generate heat by determining if the temperature rise rate of the battery is greater than the set temperature rise rate (0.03 °C/min); if the search stage is over, the system judges that the battery does not generate heat by itself and the heat wire will increase the temperature of the battery by 5 °C. The system will start the next round of the HWS mode, until it is determined that the battery self-heats or the battery temperature reaches the preset maximum experiment temperature, whereupon the test stops. The temperature sensor is arranged in the center of the battery shell during the test. Test parameter settings are shown in Table 3.

Table 2. Parameter Settings of ARC Ramp Program

serial no.	parameter	numerical value
1	chamber temperature rise rate (°C/min)	2
2	test cutoff temperature (°C)	300
3	maximum temperature of cavity (°C)	500

3. TEST RESULTS AND DATA ANALYSIS

3.1. Thermal Stability of High Nickel Cylindrical Lithium Battery Materials. The heat flow and thermogravimetric curves of the cathode material are shown in Figure 4a. There are two weight loss stages in the thermogravimetric curve. The weight loss in the first stage is between 68.77 and 158.52 °C and the weight loss ratio is 2.19%, which is caused by the thermal decomposition of the cathode electrolyte

https://doi.org/10.1021/acsomega.1c06495
ACS Omega 2022, 7, 14562−14570

Table 3. ARC HWS Program Parameter Settings

serial no.	parameter	numerical value
1	test start temperature (°C)	60
2	length of initial calibration (min)	120
3	test cutoff temperature (°C)	500
4	temperature rise step length (°C)	5
5	self-exothermic criterion (°C/min)	0.03
6	waiting time (min)	15

interface (CEI) film that formed on the cathode surface.[29] In the second stage, the weight loss is between 227.09 and 617 °C and the weight loss ratio is 14.699%, which is caused by the decomposition reaction of the cathode material to produce oxygen. An exothermic peak appears at 201.22−248.28 °C in the heat flow curve, its peak appears at 233.32 °C, and the exothermic heat is 91.44 J/g. This heat peak corresponds to the oxygen evolution reaction in the second stage of the thermogravimetric curve. The exothermic peak is caused by the decomposition reaction of the anode material to produce oxygen.

Figure 4b shows the heat flow and thermogravimetric curves of the anode. The quality of the anode material decreases significantly at 100.35−293.44 °C and is reduced by 4.4%. An exothermic peak appears at 77.13−152.52 °C in the heat flow curve, which is related to the decomposition of the SEI film. Its peak is at 111.30 °C, and the exothermic heat is 81.59 J/g. An exothermic peak of the negative electrode decomposition is observed at 319 °C.

The heat flow and thermogravimetric curves of the separator are shown in Figure 4c. The exothermic peak at 69.4 °C is caused by the thermal decomposition of $LiPF_6$.

The other two endothermic peaks are caused by the heat absorption of the separator. The melting points of the PP and PE membranes are 130 and 170 °C, respectively. The temperatures of the two peaks in Figure 4c are 135.86 and 168.59 °C, respectively, corresponding to the melting points of PP and PE.[30]

3.2. Research on Temperature Difference between Inside and Outside in the Process of Thermal Runaway.

A 100% SOC high nickel battery with a mandrel is heated through the ARC cavity at a constant rate of 2 °C/min. The heat is transferred to the battery through air convection to cause thermal runaway, and two temperature sensors arranged on the battery core and external surface record the temperature data that describes the temperature difference between inside and outside in the process of thermal runaway. Figure 5a shows the variation curve of the temperature difference between the inside and outside with the surface temperature during the thermal runaway of a 100% SOC battery. Before point A (91.84 °C), the external heating of the battery increased significantly, and the internal and external temperature difference ΔT was negative and decreased. The endothermic reaction inside the battery at point A leads to a decrease in ΔT. From point A to point B, ΔT drops quickly just after point A and then rises slowly, which may be related to the decomposition and regeneration of the SEI film. From point B to point C (160.09 °C), the fluctuation of the temperature difference ΔT between the inside and outside (an increase of 0.6 °C) may be related to the heat absorption of the diaphragm fusing. However, due to the violent reaction in this stage when the battery is fully charged, the temperature rises quickly, and the mild endothermic reaction (i.e., the melting of the diaphragm) does not have a significant effect on the temperature.

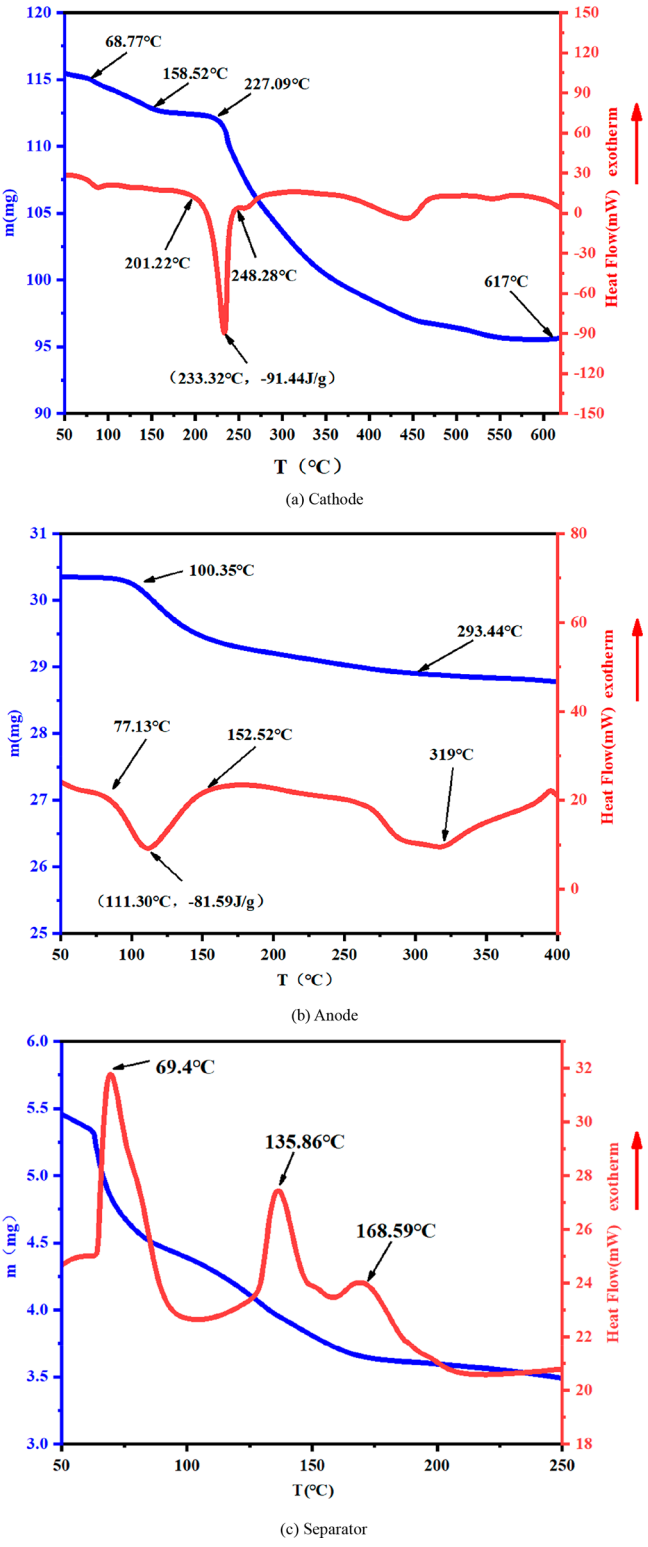

Figure 4. Heat flow and thermogravimetric curves of battery material: (a) cathode, (b) anode, and (c) separator.

To amplify the temperature change of the heat absorption for the BC section diaphragm, a 0% SOC battery was selected for internal and external temperature difference testing, as shown in Figure 5b. Battery point A also showed a decrease in the internal and external temperature difference ΔT. From

https://doi.org/10.1021/acsomega.1c06495
ACS Omega 2022, 7, 14562−14570

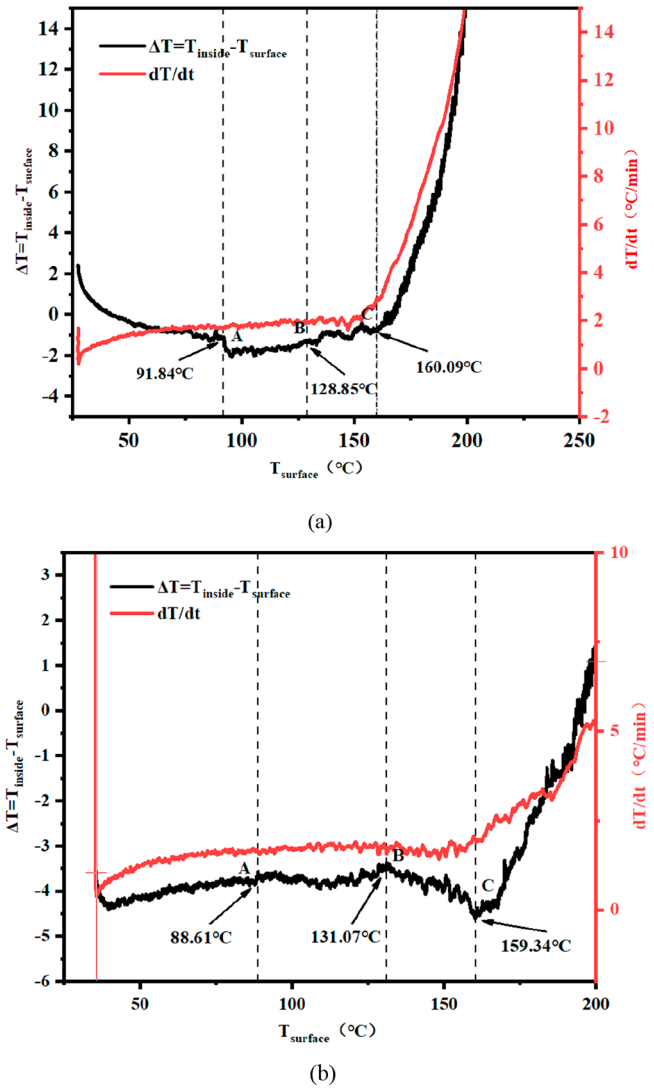

Figure 5. Temperature differences between inside and outside of thermal runaway in a high nickel battery at (a) 100% state of charge (SOC) and (b) 0% SOC.

point B (131.07 °C) to point C (159.34 °C), the temperature difference between inside and outside ΔT decreased from −3.43 to −4.62 °C, indicating a drop of 1.2 °C. The heat absorption of the diaphragm increases the temperature difference between the inside and the outside by 1.8 °C, which can further reduce the heating rate of the cavity to make the internal reaction of the battery sufficient to explore the precise heat absorption of the diaphragm. In Figure 5a, after point C, the temperature difference ΔT between the inside and outside of the battery increases sharply. This is due to a short circuit inside the battery caused by the diaphragm breakdown. The short circuit inside the battery releases a large amount of Joule heat, and the surface heating rate of the battery is much lower than that of the inner core. The short circuit of the inner core continues to heat up, triggering the reaction between the positive electrode and the electrolyte, resulting in a thermal runaway explosion. In Figure 5b, the temperature difference ΔT between the inside and outside of the 0% SOC battery after point C increases slowly. This is due to the low state of battery charge, the small heat released by the battery's internal short circuit, and its side reactions; therefore, the battery does not experience thermal runaway.

To further explore the temperature difference between inside and outside during the occurrence of thermal runaway, the temperatures inside and outside the battery are plotted in Figure 6. When the battery reaches 160.09 °C, the internal

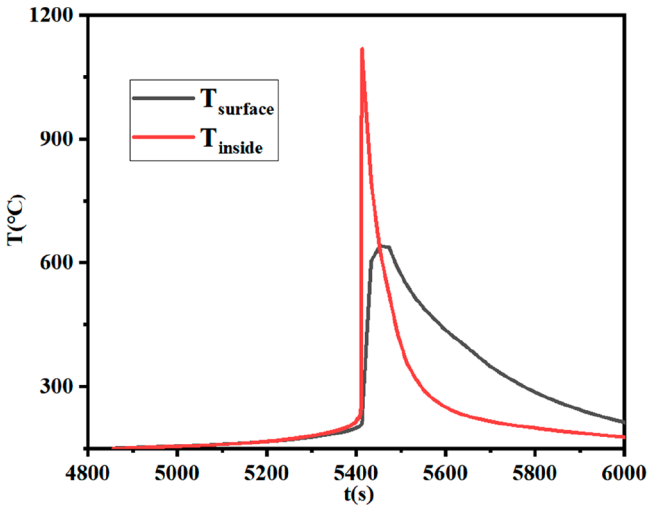

Figure 6. Temperatures of battery inside and at the surface at thermal runaway.

heat generation of the battery begins to increase appreciably. When thermal runaway occurs, the maximum temperature difference between the inside and the outside is 905 °C; at this time, the surface temperature is 212.79 °C and the inside temperature is 1117.8 °C. The maximum surface temperature is 641.41 °C, and the maximum inside temperature is 1117.8 °C. When the thermal runaway occurs, the interior of the battery heats up rapidly. At this time, the thermal insulation tape attached to the anode has been washed away by the gas generated inside the battery. There is a large temperature gradient difference between the internal and external environments, which will cause the internal temperature of the battery to drop rapidly. As the overall temperature of the battery thermal runaway further increases, the temperature sensor will eject from the battery along with the jelly roll. At this time, the temperature sensor is in the external environment and detects the ambient temperature, which causes the temperature to drop rapidly. The time difference between the maximum temperatures inside and outside the battery is 40 s. Studying the temperature difference between inside and outside the battery during thermal runaway provides guidance for the addition of flame-retardant materials inside the battery, the in-depth exploration of the spreading process, and the prevention of thermal runaway.

Previously, the detected temperature was generally the external battery temperature, and the maximum temperature range of thermal runaway of ternary batteries was 300−800 °C.[31] This inside and outside temperature difference test increases the knowledge of the maximum battery temperature. The above content takes the NCM811 battery as an example and calculates the heat released from the battery during thermal runaway according to $E = c \cdot m \cdot \Delta T$, where c represents the specific heat capacity of the battery, which is taken as 1 J/(g·K); m represents the mass (g) of the battery; and ΔT represents the temperature difference of the battery. From the

https://doi.org/10.1021/acsomega.1c06495
ACS Omega 2022, 7, 14562−14570

battery thermal runaway trigger temperature T_c to the thermal runaway maximum temperature T_m stage, the heat released from the battery thermal runaway is 25.73 kJ, which is equivalent to a 5.8 g TNT explosion (15% TNT equivalent 4.437 kJ/g). By contrast, the battery thermal runaway heat release of 48.22 kJ, equivalent to a 10.8 g TNT explosion (calculated at the maximum inside temperature of the battery), is about 1.87 times higher than the perception of the energy released by the explosion.

3.3. High Nickel Cylindrical Lithium Battery Cell High-Temperature Thermal Runaway. The thermal runaway process of the 100% SOC battery is investigated through the ARC's HWS program. We define the self-generated heat temperature T_0 when the rate of increase of battery temperature is continuously greater than 0.03 °C/min, the temperature at which the battery safety valve ruptures is T, the temperature at which the battery separator melts and causes a sudden voltage drop is T_d, and the temperature at which the battery thermal runaway is triggered is T_c when the rate of increase of battery temperature is continuously greater than 1 °C/s. The maximum temperature that can be reached during the thermal runaway explosion is T_m.

During the thermal runaway process of the battery, the changes in temperature, voltage, and increase in the rate of the temperature of the battery are shown in Figure 7. The battery

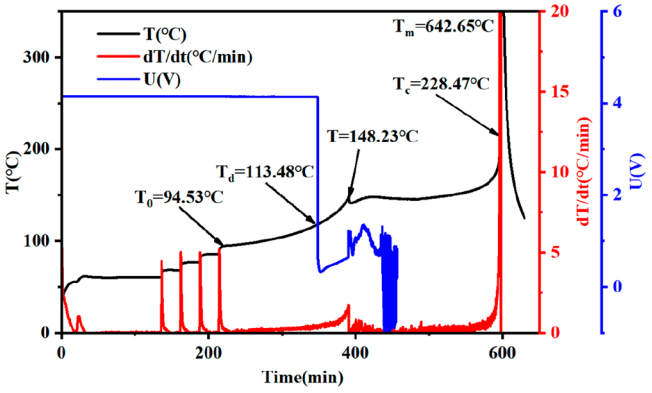

Figure 7. Temperature, temperature rise rate, and voltage variation during the high-temperature thermal runaway of a battery cell.

was heated to 60 °C, and after 2 h of temperature control, no self-generated heat was detected in the battery. The battery was then heated according to the gradient. With the increase in battery temperature, SEI film will be heated and decomposed to release heat. When the temperature rise rate of the battery is continuously greater than or equal to 0.03 °C/min, self-generated heat begins to occur and the starting temperature of the battery's self-generated heat T_0 is 94.53 °C. With the increase in battery temperature, the local heating shrinkage of the battery separator causes a micro short circuit in the battery, and the battery voltage will drop to near zero rapidly.

The drop temperature T_d is 113.48 °C. At this time, the partial micro short circuit of the separator does not appear as a large area fuse, and the separator closes the Li^+ transmission channel, leading to the voltage drop. The micro short circuit of the battery and the continuous decomposition of SEI film will produce gas, which will cause the pressure inside the battery to rise and break through the pressure reducing valve. The breaking temperature of the pressure relief valve T is 148.23 °C. The gas breaks through the pressure relief valve and takes some heat from the battery body, causing the battery temperature to drop briefly. After the pressure relief valve breaks down, the active substance inside the battery contacts air directly, aggravating the reaction of the internal material and causing the battery temperature to continue to rise. When the temperature rise rate of the battery reaches 1 °C/s, the temperature T_c of the battery thermal runaway trigger is 228.47 °C. At this time, the temperature on the surface of the battery increases exponentially, and the cathode material decomposition and oxygen precipitate react with the electrolyte, aggravating the runaway contact heating of the battery, causing fire and explosion. The maximum thermal runaway temperature T_m of the battery is 642.65 °C.

Combined with the thermal stability of the battery material and the thermal runaway of the battery cell at high temperature, the process of battery thermal runaway is summarized by the following five processes:

I. From 0 to 94.53 °C: The battery is in a safe state, and no other self-heating reaction occurs.
II. From 94.53 to 113.48 °C: Heat is derived from the decomposition of the SEI membrane.
III. From 113.48 to 168.59 °C: The separator shrinks at 113.48 °C, melts at 135.86 °C, and collapses at 168.59 °C. The scope of the internal short circuit is gradually expanded, causing the voltage to drop.
IV. From 168.59 to 228.47 °C: The separator large area collapse causes a large amount of Joule heat to be released by a short circuit in a large area but does not lead directly to thermal runaway. The heat in this stage mainly comes from the Joule heat released by the short circuit.
V. From 228.47 °C to fire and explosion: When the decomposition temperature of the cathode material is reached, the cathode material separates oxygen and reacts with the electrolyte, thereby releasing a large amount of heat and causing battery thermal runaway.

The sequence diagram of battery thermal runaway is summarized in Figure 8. During the battery thermal runaway

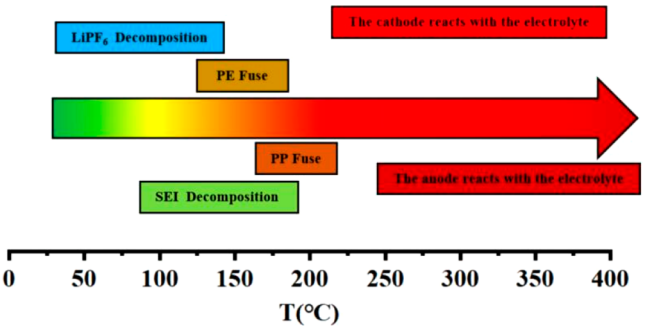

Figure 8. Thermal runaway process.

process, $LiPF_6$ pyrolysis, SEI film decomposition and regeneration reaction, PE diaphragm fusing, PP diaphragm fusing, cathode decomposition and electrolyte reaction, anode decomposition and electrolyte reaction, etc. occur.

The detected battery thermal runaway trigger temperature by the outer thermocouple is 228.47 °C, and the battery consistency is good. According to the internal and external temperature difference test during the battery thermal runaway process, the internal temperature of the battery is 1117.8 °C

https://doi.org/10.1021/acsomega.1c06495
ACS Omega 2022, 7, 14562−14570

when the battery reaches the thermal runaway trigger temperature, which has reached the highest temperature. The battery cathode material begins to decompose around 227.09 °C. It takes 5.75 s from the inside of the battery to reach the decomposition temperature of the cathode material to the external monitoring to the triggering temperature of the battery's thermal runaway. It can be seen that when the thermal runaway trigger is detected at the outside of the battery, irreversible damage has occurred inside the battery.

4. RESULTS AND DISCUSSION

Using the STA8000 and ARC, the thermal stability of 100% SOC NCM811 battery materials and the thermal runaway process of a cell at a high temperature were studied. The thermal runaway process of a battery at high temperature was revealed by the thermal performance of its cathode, anode, and separator. The main conclusions are as follows:

1. The cathode material decomposed around 227.09 °C, releasing 91.44 J/g. The SEI decomposed and anode material reacted with the electrolyte at 77.13−152.52 °C, releasing 81.59 J/g. The separator melted and collapsed at 135.86 and 168.59 °C, respectively, due to the melting of PE and PP materials.

2. A high nickel battery with a mandrel was used to explore the temperature difference between inside and outside the battery during thermal runaway. Heat generation inside the battery began to increase during thermal runaway (when the battery reached 169.09 °C), and a large number of exothermic chemical reactions started to occur inside the battery that resulted in a rapid increase in the temperature difference between inside and outside the battery. The maximum temperature difference between inside and outside was 905 °C; when that difference was reached, the surface temperature was 212.79 °C and the inside temperature was 1117.8 °C. The time difference between the maximum temperature inside and outside the battery is 40 s. The heat released from the thermal runaway of a high nickel battery is 48.22 kJ (equivalent to 10.8 g of TNT explosion), increasing the perception of energy released from the explosion by about 1.87 times.

3. The thermal runaway onset temperature of the high nickel battery monomer was 94.53 °C, which was caused by the initial decomposition of SEI film and the heat release in combination with the thermal stability analysis of the battery material. The thermal runaway trigger temperature was 228.47 °C, which was mainly contributed by the reaction between the anode and electrolyte, releasing Joule heat from an internal short circuit of the cathode and anode electrode as well as the reaction between the cathode and electrolyte. The maximum temperature of the thermal runaway process was 642.65 °C, with a maximum temperature rise rate of 579.43 °C/min, which was caused mainly by the reaction between the oxygen precipitated from the decomposition of the cathode material and the electrolyte.

AUTHOR INFORMATION

Corresponding Authors

Zuoqiang Dai − *College of Mechanical and Electrical Engineering, Qingdao University, Qingdao 266071, China; Engineering Technology Center of Power Integration and Energy Storage System, Qingdao University, Qingdao 266071, China*; Email: daizuoqiangqdu@163.com

Lili Zheng − *College of Mechanical and Electrical Engineering, Qingdao University, Qingdao 266071, China; Engineering Technology Center of Power Integration and Energy Storage System, Qingdao University, Qingdao 266071, China*; Email: llzhengqdu@163.com

Authors

Longzhou Jia − *College of Mechanical and Electrical Engineering, Qingdao University, Qingdao 266071, China; Engineering Technology Center of Power Integration and Energy Storage System, Qingdao University, Qingdao 266071, China*; orcid.org/0000-0001-7642-7658

Dong Wang − *College of Mechanical and Electrical Engineering, Qingdao University, Qingdao 266071, China; Engineering Technology Center of Power Integration and Energy Storage System, Qingdao University, Qingdao 266071, China*

Tao Yin − *College of Mechanical and Electrical Engineering, Qingdao University, Qingdao 266071, China; Engineering Technology Center of Power Integration and Energy Storage System, Qingdao University, Qingdao 266071, China*; orcid.org/0000-0003-4840-5384

Xichao Li − *Energy Saving Business Division, CRRC Qingdao Sifang Rolling Stock Research Institute Co. Ltd., Qingdao 266031, China*

Liwei Li − *School of Control Science and Engineering, Shandong University, Jinan 250061, China*

Complete contact information is available at: https://pubs.acs.org/10.1021/acsomega.1c06495

Notes

The authors declare no competing financial interest.

ACKNOWLEDGMENTS

The authors gratefully acknowledge financial support from the National Key Research and Development Program of China under Grant 2017YFB0102004 and Natural Science Foundation of Shandong Province under Grant ZR2020ME019.

REFERENCES

(1) Feng, X. N.; Fang, M.; He, X. M.; Ouyang, M. G.; Lu, L. G.; Wang, H.; Zhang, M. Thermal runaway features of large format prismatic lithium ion battery using extended volume accelerating rate calorimetry. *J. Power Sources.* **2014**, *255*, 294−301.

(2) Duh, Y. S.; Tsai, M. T.; Kao, C. S. Thermal runaway on 18650 lithium-ion batteries containing cathode materials with and without the coating of self-terminated oligomers with hyper-branched architecture (STOBA) used in electric vehicles. *J. Therm. Anal. Calorim.* **2017**, *129*, 1935−1948.

(3) Wang, Q. S.; Mao, B. B.; Stoliarov, S. I.; Sun, J. H. A review of lithium-ion battery failure mechanisms and fire prevention strategies. *Prog. Energy Combust. Sci.* **2019**, *73*, 95−131.

(4) Liu, B. H.; Jia, Y. K.; Yuan, C. H.; Wang, L. B.; Gao, X.; Yin, S.; Xu, J. Safety issues and mechanisms of lithium-ion battery cell upon mechanical abusive loading: A review. *Energy Stor. Mater.* **2020**, *24*, 85−112.

(5) Feng, X. N.; Zheng, S. Q.; He, X. M.; Wang, L.; Ren, D. S.; Ouyang, M. G.; Wang, Y. Time sequence map for interpreting the thermal runaway mechanism of lithium-ion batteries with LiNixCoyMnzO2. *Front. Energy Res.* **2018**, *6*, 126.

(6) Feng, X. N.; Ouyang, M. G.; Liu, X.; Lu, L. G.; Xia, Y.; He, X. M. Thermal runaway mechanism of lithium ion battery for electric vehicles: A review. *Energy Stor. Mater.* **2018**, *10*, 246−267.

(7) Jiang, X. Y.; Zhu, X. M.; Ai, X. P.; Yang, H. X.; Cao, Y. L. Novel Ceramic-Grafted separator with highly thermal stability for safe lithium-ion batteries. *ACS Appl. Mater. Interfaces.* **2017**, *9*, 25970−25975.

(8) Wang, Q. S.; Sun, J. H.; Chen, C. H. Thermal stability of LiPF6/EC+DMC+EMC electrolyte for lithium ion batteries. *Pare Metals.* **2006**, *25*, 94−99.
(9) Maleki, H.; Deng, G. P.; Anani, A.; Howard, J. Thermal stability studies of Li-ion cells and components. *J. Electrochem. Soc.* **1999**, *146*, 3224−3229.
(10) Richard, M. N.; Dahn, J. R. Accelerating rate calorimetry study on the thermal stability of lithium intercalated graphite in electrolyte I. Experimenta. *J. Electrochem. Soc.* **1999**, *146*, 2068−2077.
(11) Spotnitz, R.; Franklin, J. Abuse behavior of high power, lithium-ion cells. *J. Power Sources.* **2003**, *113*, 81−100.
(12) Liu, X.; Ren, D. S.; Hsu, H. J.; Feng, X. N.; Xu, G. L.; Zhuang, M. H.; Gao, H.; Lu, L. G.; Han, X. B.; Chu, Z. Y.; et al. Thermal runaway of lithium-ion batteries without internal short circuit. *Joule.* **2018**, *2*, 2047−2064.
(13) Roth, E. P.; Doughty, D. H. Thermal abuse performance of high-power 18650 Li-ion cells. *J. Power Sources.* **2004**, *128*, 308−318.
(14) Doughty, D. H.; Roth, E. P.; Crafts, C. C.; Nagasubramanian, G.; Henriksen, G.; Amine, K. Effects of additives on thermal stability of Li ion cells. *J. Power Sources.* **2005**, *146*, 116−120.
(15) Golubkov, A. W.; Fuchs, D.; Wagner, J.; Wiltsche, H.; Stangl, C.; Fauler, G.; Voitic, G.; Thaler, A.; Hacker, V. Thermal runaway experiments on consumer Li-ion batteries with metal-oxide and olivin-type cathodes. *RCS Adv.* **2014**, *4*, 3633−3642.
(16) Ping, P.; Wang, Q. S.; Huang, P. F.; Li, K.; Sun, J. H.; Kong, D. P.; Chen, C. H. Study of the fire behavior of high-energy lithium-ion battery with full-scaled burning test. *J. Power Sources.* **2015**, *285*, 80−89.
(17) Kong, D. P.; Wang, G. Q.; Ping, P.; Wen, J. Numerical investigation of thermal runaway behavior of lithium-ion batteries with different battery materials and heating conditions. *Appl. Therm. Eng.* **2021**, *189*, 116661.
(18) Jhu, C. Y.; Wang, Y. W.; Wen, C. Y.; Chiang, C. C.; Shu, C. M. Self-reactive rating of thermal runaway hazards on 18650 lithium-ion batteries. *J. Therm. Anal. Calorim.* **2011**, *106*, 159−163.
(19) Duh, Y. S.; Tsai, M.; Kao, C. S. Thermal runaway on 18650 lithium-ion batteries containing cathode materials with and without the coating of self-terminated oligomers with hyper-branched architecture (STOBA) used in electric vehicles. *J. Therm. Anal. Calorim.* **2017**, *129*, 1935−1948.
(20) Zhu, L.; Xu, X. M.; Zhao, L.; Yuan, Q. Q. Comparative analysis of thermal runaway characteristics of lithium-ion battery under oven test and local high temperature. *Fire Mater.* **2022**, *46*, 397.
(21) Sun, Y.; Ren, D. S.; Liu, G. J.; Mu, D. B.; Wang, L.; Wu, B. R.; Liu, J. H.; Wu, N. N.; He, X. M. Correlation between thermal stabilities of nickel-rich cathode materials and battery thermal runaway. *Int. J. Energy Res.* **2021**, *45*, 20867−20877.
(22) Li, H.; Chen, H. D.; Zhong, G. B.; Wang, Y.; Wang, Q. S. Experimental study on thermal runaway risk of 18650 lithium ion battery under side-heating condition. *J. Loss Prev. Process Ind.* **2019**, *61*, 122−129.
(23) Li, Y.; Liu, X.; Wang, L.; Feng, X. N.; Ren, D. S.; Wu, Y.; Xu, G. L.; Lu, L. G.; Hou, J. X.; Zhang, W. F.; et al. Thermal runaway mechanism of lithium-ion battery with LiNi0.8Mn0.1Co0.1O2 cathode materials. *Nano Energy.* **2021**, *85*, 105878.
(24) Liu, J. J.; Wang, Z. R.; Gong, J. H.; Liu, K.; Wang, H.; Guo, L. S. Experimental Study of Thermal Runaway Process of 18650 Lithium-Ion Battery. *Materials* **2017**, *10*, 230.
(25) Zhang, P. H.; Yuan, W.; Wei, Z. Y.; Li, Z. J. Thermal runaway analysis of NCM lithium-ion battery in humid and hot environment. *Dongbei Daxue Xuebao, Ziran Kexueban* **2020**, *41*, 881−887.
(26) Wang, H. B.; Du, Z. M.; Rui, X. Y.; Wang, S. Y.; Jin, C. Y.; He, L.; Zhang, F. S.; Wang, Q. Z.; Feng, X. N. A comparative analysis on thermal runaway behavior of Li(NixCoMnz)O-2 battery with different nickel contests at cell and module level. *J. hazard. Mater.* **2020**, *393*, 122361.
(27) Wang, D.; Zheng, L. L.; Li, X. C.; Du, G. C.; Feng, Y.; Jia, L. Z.; Dai, Z. Q. Thermal safety of ternary soft pack power lithium battery. *Chuneng Kexue Yu Jishu* **2020**, *9*, 1517−1525.
(28) Zhao, C. P.; Sun, J. H.; Wang, Q. S. Thermal runaway hazards investigation on 18650 lithium-ion battery using extended volume accelerating rate calorimeter. *J. Energy Storage.* **2020**, *28*, 101232.
(29) Wursig, A.; Buqa, H.; Holzapfel, M.; Krumeich, F.; Novak, P. Film formation at positive electrodes in lithium-ion batteries. *Electrochem. Solid-State Lett.* **2005**, *8*, A34−A37.
(30) Aurbach, D. Electrode-solution interactions in Li-ion batteries: a short summary and new insights. *J. Power Sources.* **2003**, *119*, 497−503.
(31) Wang, G. W.; Zhang, S.; Li, M.; Wu, J. J.; Wang, B.; Song, H. Deformation and failure properties of high-Ni Lithium-Ion battery under axial loads. *Materials* **2021**, *14*, 7844.

https://doi.org/10.1021/acsomega.1c06495
ACS Omega 2022, 7, 14562−14570